

1 **The changing character of twenty-first century precipitation over the**
2 **western United States in the variable-resolution CESM**

3 Xingying Huang, * Paul A. Ullrich

4 *Department of Land, Air and Water Resources, University of California, Davis*

5 *Corresponding author address: Xingying Huang, Department of Land, Air and Water Resources,
6 University of California Davis, Davis, CA 95616.
7 E-mail: xyhuang@ucdavis.edu

ABSTRACT

8 (To be added once the main content settled down)

9 **1. Introduction**

10 Understanding the character of precipitation within a changing climate has a major focus of
11 climate science, primarily due to the pronounced impacts of water availability on socioeconomic
12 and natural systems (Hegerl et al. 2004; Kharin et al. 2007; Scoccimarro et al. 2013). Among
13 these studies, there has been particular interest in precipitation extremes, which are manifested as
14 drought and heavy precipitation events (Seneviratne et al. 2012). Studies examining the charac-
15 ter of precipitation in a warming world, which utilize models of varying complexity from simple
16 thermodynamic models through complex coupled climate simulations, suggest that although at-
17 mospheric water vapor is increasing, the associated impacts of increased atmospheric water vapor
18 on precipitation are far more complicated. Extreme precipitation events are even more nuanced:
19 Some studies suggest that the intensity of extreme precipitation is projected to increase under
20 global warming in many parts of the world, even in the regions where mean precipitation decreases
21 (Tebaldi et al. 2006; Kharin et al. 2007).

22 Although future climate predictions are known to be often associated with large uncertainties,
23 climate models are nonetheless one of the most useful tools for studying climate variability and ex-
24 tremes events in the future (Easterling et al. 2000). Global climate models (GCMs) are often used
25 to investigate possible future changes in the mean, variability and extremes of climate, typically
26 forced with predicted greenhouse gas (GHGs) concentrations and aerosol emissions. Precipitation
27 extremes, as measured by various metrics, are predicted to change by future warming based on the
28 results of these simulations (Meehl et al. 2006). Several past studies have investigated global im-
29 pacts (Seneviratne et al. 2012), but impacts at local and regional scales are more difficult to come
30 by. Although increased GHG concentrations have contributed to observed intensification of heavy
31 precipitation events over the tropical ocean (Allan and Soden 2008) and the majority of Northern

³² Hemisphere overland areas Min et al. (2011), these impacts are much more poorly understood at
³³ regional scales due to atmospheric circulation patterns of variability (Trenberth 2011), which are
³⁴ more difficult to assess at the coarse model resolutions used in previous studies.

³⁵ Insufficient regional-scale climate information has been a major outstanding problem in climate
³⁶ science, as stakeholders and water managers typically require fine-scale information on climate
³⁷ impacts in order to effectively develop adaptation and mitigation strategies. In order to reach the
³⁸ scales needed for effective local planning, dynamical downscaling with regional climate models
³⁹ (RCMs) has been typically used to ascertain the frequency, intensity, and duration of extreme
⁴⁰ events. By only simulating a limited regional domain, RCMs better capture fine-scale dynami-
⁴¹ cal features under high horizontal resolution (Bell et al. 2004; Frei et al. 2006; Rauscher et al.
⁴² 2010; Wehner 2013). Higher resolution can also enable more accurate simulations of precipitation
⁴³ extremes, which can be driven by land use, land/water contrast, snow cover, cloudiness and circu-
⁴⁴ lation patterns associated with topography (Leung et al. 2003a; Diffenbaugh et al. 2005; Salathé Jr
⁴⁵ et al. 2008; Wehner et al. 2010). Diffenbaugh et al. (2005) studied both heat events and wet events
⁴⁶ over the contiguous United States based on RCMs simulation at 25 km horizontal resolution, and
⁴⁷ demonstrated that fine-scale processes are critical for accurate assessment of local- and regional-
⁴⁸ scale climate change vulnerability. Leung et al. (2003b) showed that the higher-resolution nests
⁴⁹ utilized by RCMs yield more realistic precipitation patterns and produce more frequent heavy
⁵⁰ precipitation over the western U.S. (WUS), which is in turn more consistent with observations.

⁵¹ Despite their success, RCMs also have known issues associated with inconsistency between the
⁵² lateral forcing data and the driven RCM, and the menu of physical parameterizations typically
⁵³ available to RCMs expose the potential for over-tuning the model for a particular geographic
⁵⁴ region (McDonald 2003; Laprise et al. 2008; Mesinger and Veljovic 2013). Consequently, there
⁵⁵ has been growing interest in variable-resolution enabled GCMs (VRGCMs) to improve regional

56 climate simulations. Unlike RCMs, which require GCM data to drive the simulation at lateral
57 boundaries, VRGCMs use a unified model with coarse global resolution and enhanced resolution
58 over a specific study region (Staniforth and Mitchell 1978; Fox-Rabinovitz et al. 1997). VRGCMs
59 have demonstrated comparable utility for regional climate studies at a reduced computational cost,
60 particular when compared to uniform-resolution GCMs (Fox-Rabinovitz et al. 2006; Rauscher
61 et al. 2013).

62 In this paper, we utilize the recently developed variable-resolution option in the Community
63 Earth System Model (VR-CESM). VR-CESM is based on the CESM (and its predecessor, the
64 Community Climate System Model (CCSM)), a family of models that have been used for decades
65 to study the global climate (Neale et al. 2010a; Hurrell et al. 2013), and demonstrated competitive
66 ability when contrasted with other climate models. The overall performance of VR-CESM for
67 modeling regional climate in the California and Nevada is detailed in Huang et al. (2016), who
68 argued VR-CESM has competitive biases in comparison to the Weather Research and Forecast-
69 ing (WRF) model (a traditional RCM), when evaluating both against high-quality observations
70 and reanalysis. VR-CESM has also been employed for other studies and demonstrated that it is
71 competitive at capturing fine-scale atmospheric processes with the uniform-resolution CESM and
72 other RCMs, without apparent artifacts within the coarse-fine transition region (Zarzycki et al.
73 2014, 2015; Rhoades et al. 2015).

74 This study focuses changes in the character of precipitation over the 21st Century within the
75 WUS, as predicted from long-term ensemble runs conducted with VR-CESM with a local grid
76 resolution of $\sim 0.25^\circ$. The WUS is known to be particularly vulnerable to hydrological extreme
77 events, particularly floods and droughts (Leung et al. 2003b; Caldwell 2010), and features a variety
78 of local features and microclimates associated with its rough and varied topography. Simulations
79 of the future climate are performed in accordance with the representative concentration pathway

80 (RCP) 8.5 scenario, which describes a “business-as-usual” projection for GHGs among other RCPs
81 (Riahi et al. 2011). RCP 8.5 is a baseline scenario with updated base year calibration (to 2005)
82 and no explicit climate policy (Riahi et al. 2011) and end-of-century projections with the substan-
83 tially weaker RCP2.6 scenario are found to be qualitatively similar to mid-century RCP8.5 results.
84 Simulations are further conducted in accordance with the Atmospheric Model Intercomparison
85 Project (AMIP) protocol (Gates 1992), a widely-used approach for climate model diagnosis, val-
86 idation and intercomparison that imposes global sea surface temperatures (SSTs) and sea ice. By
87 constraining atmospheric boundary conditions at the sea surface, we avoid model biases that are
88 known to exist in the fully coupled configuration (??) and accept potential uncertainties associated
89 with our choice of SSTs.

90 Changes in the character of precipitation, in terms of frequency and intensity, have been assessed
91 in our study from recent history through the end of 21st century. A comprehensive set of metrics
92 for precipitation extremes have been evaluated from ensemble simulations over the **26-year** peri-
93 ods corresponding to historical (1980-2005), mid-century (2025-2050) and end-of-century (2075-
94 2100). Using this information, it is our goal to improve our understanding of precipitation at
95 relatively fine spatial scales. We hypothesize that spatial inhomogeneity in local geography and
96 temperature will also result in similarly inhomogeneous impacts on the precipitation field. We fur-
97 ther expect that teleconnections (specifically the El Niño-Southern Oscillation (ENSO)) will have
98 a pronounced impact on precipitation features over particular area under the changes of mean SST
99 and its variations. Since only one SST dataset was used for this study, we note that our projections
100 are conditioned on a particular future character of ENSO. This is a potentially large source of
101 uncertainty, as at present there is no clear consensus on how ENSO may behave under a warming
102 climate (Fedorov and Philander 2000; Guilyardi et al. 2009), and strengthening or weakening of
103 this pattern will have clear consequences for our results.

104 This work builds on a number of previous studies that have explored the projected future change
105 in WUS precipitation. For example, Kim (2005) applied downscaled climate change signals to se-
106 lected indicators, and concluded that global warming induced by increased CO₂ is likely to drive
107 increases in extreme hydrologic events in the WUS. Duffy et al. (2006) found that mean precip-
108 itation predicted by the RCMs are not statistically significant compared to interannual variability
109 in many regions over WUS, though there is little consistency among the different RCMs as to
110 responses in precipitation to increased GHGs. Gao et al. (2015) pointed out a potentially large
111 increase in atmospheric river events by the end of the 21st century under the RCP8.5 scenario.

112 This paper is structured as follows. Section 2 describes the model setup. Section 3 describes
113 the methodology and reference datasets employed. An assessment of the ability of the model to
114 capture the climatology of the WUS is given in section 4. Results from the future mean climatol-
115 ogy trend and projected changes to precipitation indices is in section 6. Section 7 summarizes the
116 main points of the study along with further discussions.

117 2. Model Setup

118 CESM is a state-of-the-art Earth modeling framework, consisting of coupled atmosphere, ocean,
119 land and sea ice models (Neale et al. 2010b; Hurrell et al. 2013). In this study, Community At-
120 mosphere Model version 5 (CAM5) (Neale et al. 2010b) and the Community Land Model version
121 4.0 (Oleson et al. 2010) are used. Within CAM5, we use the Spectral Element (SE) dynamical
122 core, which incorporates the variable-resolution option (Zarzycki et al. 2014) and includes de-
123 sirable conservation and parallel scalability properties (Dennis et al. 2011; Taylor 2011). CLM
124 is employed in the *unigrid* configuration, which allows the land model to be co-located with the
125 atmospheric grid and so eliminates the need for interpolation. SSTs and sea ice, which are used
126 to compute ocean-atmosphere fluxes, are prescribed in accordance with the AMIP protocol (Gates

¹²⁷ 1992). The variable-resolution mesh used for this study is depicted in Figure 1, in accord with our
¹²⁸ past studies (Rhoades et al. 2015; Huang et al. 2016; ?).

¹²⁹ Simulations have been performed for the historical period (1979-2005, hereafter referred to as
¹³⁰ hist) and for two future periods: 2024-2050 (hereafter referred to as mid) and 2074-2100 (hereafter
¹³¹ referred to as end). For purposes of analysis, the first year of each time period was discarded as a
¹³² spin-up period to allow adequate time for the initialized land and atmosphere to equilibrate. The
¹³³ 26-year duration was chosen to provide an adequate sampling of annual variability for each time
¹³⁴ phase. For future projections, GHG concentrations are set based on RCP8.5. Historical SSTs and
¹³⁵ sea ice are prescribed at 1° resolution, as described by Hurrell et al. (2008). SSTs and sea ice
¹³⁶ for each future period are developed from fully-coupled RCP 8.5 climate simulations with bias
¹³⁷ correction applied (Cecile Hannay, personal communication). Using prescribed SSTs in place of
¹³⁸ a coupled ocean model considerably reduces the computation cost and so allows the atmospheric
¹³⁹ model to be run at a higher overall resolution. Annually-updated land surface datasets, which
¹⁴⁰ prescribe land-use characteristics, are interpolated from 0.5° to the land model grid.

¹⁴¹ Ensemble runs are needed to ensure that the sample adequately accounts for climate variability,
¹⁴² especially for statistics associated with climatological extremes. However, the exact number of
¹⁴³ ensemble members required is heavily dependent on the variability of the particular metric being
¹⁴⁴ examined, and so no standard ensemble criteria exists (Deser et al. 2012b). Deser et al. (2012b)
¹⁴⁵ suggest that around 3 ensemble runs are required to detect a significant epoch difference for JJA
¹⁴⁶ (June-July-August) surface temperatures, whereas 10 to 30 ensemble members are needed for that
¹⁴⁷ for DJF (Dec.-Jan.-Feb.) precipitation. In our study, the use of prescribed SSTs does reduce the
¹⁴⁸ intrinsic variability of the climate system (see supplement), and so we found reasonably converged
¹⁴⁹ results with two ensemble members for the historical period and four ensemble members for each
¹⁵⁰ future period.

151 **3. Methodology**

152 *a. Precipitation indices*

153 In order to fully account for the precipitation distributions, daily output over all the years are
154 utilized in data analysis. We have employed standard indices to characterize precipitation (Tebaldi
155 et al. 2006; Zhang et al. 2011; Sillmann et al. 2013). Several indices have been examined, includ-
156 ing those defined by the Expert Team on Climate Change Detection and Indices (ETCCDI) (?) that
157 have been primarily adopted in previous studies (?Sillmann et al. 2013; Diffenbaugh et al. 2005;
158 Singh et al. 2013) and others such as return levels, dry spell and wet spell defined by either per-
159 centiles or by selected thresholds. As a result, loosely based on the former studies, the indices we
160 have chosen for this study attempt to provide a relatively comprehensive characterization of pre-
161 cipitation, along with being easy to interpret and relevant to stakeholders. The indices employed
162 are summarized in Table 1.

163 *b. Impacts of ENSO*

164 The impact of ENSO on precipitation is emphasized in our study due to its impact in regulating
165 the precipitation over a majority of our study area, particularly in the southwest U.S. (Cayan et al.
166 1999; Zhang et al. 2010; Deser et al. 2012a; Yoon et al. 2015). The phase of ENSO (*i.e.* El
167 Niño and La Niña) is identified each year using the Oceanic Niño Index (ONI), defined as the
168 3-month running means of SST anomalies in the Niño 3.4 region (covering 5N-5S, 120-170W
169 based on NOAA (2013)). An El Niño or La Niña episode is said to occur when the ONI exceeds
170 +0.5 or -0.5 for at least five consecutive months (NOAA 2013) (see the supplement). In order
171 to remove the trend in the SST field associated with climate change, the anomaly is computed
172 against the detrended mean SSTs from the periods 1971-2000, 2020-2050 and 2070-2100 for hist,

173 mid and end respectively, using the aforementioned observed and predicted SST datasets. We
174 have also tried to use wider ranges (from 105W to 170W) than 3.4 region (from 120W to 170W)
175 to recalculate the SST anomaly as argued by some studies for different types of ENSO (Kao and
176 Yu 2009), and the results are statistically the same as using Niño 3.4.

177 Student's t-test has been used to test whether or not two datasets at each grid point are statis-
178 tically equivalent, if the sample population can be adequately described by a normal distribution.
179 The normality of a dataset is assessed under the Anderson-Darling test. When the sample popu-
180 lations do not approximately follow a normal distribution, Mann-Whitney-Wilcoxon (MWW) test
181 is employed in lieu of the t-test. All these tests are evaluated at the 0.05 (α) significance level.

182 (add description of the supplement like what are included; see the sst_enso.pdf, mask the land
183 (over land, it should be the surface temperature.))

184 *c. Reference datasets*

185 Gridded observational datasets and reanalysis of the highest available quality with comparable
186 horizontal resolutions to our VR-CESM simulations are used for assessing the simulation qual-
187 ity. The use of multiple reference datasets is necessary due to the underlying uncertainty in the
188 reference data. Descriptions of the datasets employed are as follows.

189 **UW Precipitation Dataset:** The UW daily gridded meteorological data is obtained from the
190 Surface Water Modeling group at the University of Washington (Maurer et al. 2002; Hamlet
191 and Lettenmaier 2005). UW incorporates topographic corrections for the precipitation. The
192 dataset is provided at 0.125° horizontal resolution covering the period 1949 to 2010.

193 **NCEP CPC:** This dataset provides gauge-based analysis of daily precipitation from the Na-
194 tional Oceanic and Atmospheric Administration (NOAA) Climate Prediction Center (CPC).

195 It is a suite of unified precipitation products obtained by combining all information avail-
196 able at CPC via the optimal interpolation objective analysis technique. The gauge analysis
197 covers the Conterminous United States with a fine-resolution at 0.25° from 1948-01-01 to
198 2006-12-31.

199 **North American Regional Reanalysis (NARR):** The is the NCEP (National Centers for En-
200 vironmental Prediction) high-resolution reanalysis product that provides dynamically down-
201 scaled data over North America at ~ 32 km resolution and 3-hourly intervals from 1979
202 through present (Mesinger et al. 2006).

203 4. Model Assessment

204 Before proceeding, we first investigate how well the model is able to represent the character
205 of precipitation over the WUS. Figures 2 and Figure 3 depict the spatial character of the indices
206 defined in Table 1. Considering the uncertainty within the reference datasets, the mean of the ref-
207 erences are used to get the difference from the model output. T-test is applied here with UW, CPC
208 and NARR as the three statistical samples and the historical runs as two samples averaged over
209 the whole period, determining at each spatial point whether VR-CESM is statistically equivalent
210 to the references as stippled in 2 and 3.

211 Compared with observations, VR-CESM well represents the spatial pattern of precipitation, with
212 majority of the precipitation distributed along the northwest coastal area and the mountainous re-
213 gions of the Cascades and the Sierra Nevada. Compared to the mean of the references, VR-CESM
214 does overestimate the Pr significantly over most of the relatively dry region for about 0.2 mm to
215 1.5 mm, especially over the eastern side of the Cascades and both sides of the Sierra Nevada (with
216 relatively difference reaching 50%-150%). This is further reflected in the overestimation of the
217 non-extreme Pr events frequency (with $Pr < 10\text{mm/day}$) since most precipitation over dry area

is associated with low rainy rate days. However, for the western flank of the Sierra Nevada, the overestimation of the mean Pr is mainly due to the intensified rain rate, which may related with the strengthened treatment of orographic effects with excessively strong upward winds. Nonetheless, the model captures the precipitation features including frequency and intensity satisfactorily over the main wet region, where most precipitation is resulted from extreme Pr events (when $\text{Pr} > 10 \text{mm/day}$), without significant difference.

The corresponding contribution fraction to total precipitation amount of each range defined in our metrics is also well represented in the model without significant difference, except the western side of the the Sierra Nevada and eastern flank of the Cascades in the Washington. This suggests that despite the aforementioned biases, VR-CESM can still capture the overall shape of the precipitation distributions. Biases in simulating extreme precipitation over the topographically complex regions including the Cascades and Sierra Nevada ranges have also been found by in the high-resolution simulation by RCMs ?Singh et al. (2013), and have been primarily attributed to excessively strong winds. **Biases with the excessively dry eastern flanks of these mountains may also be associated with the prognostic treatment of precipitation species in CESM.**

As further supported in Huang et al. (2016) by evaluating VR-CESM also at 0.25° for long-term regional climate modeling over California, it is found that VR-CESM can adequately represented regional climatological patterns with high spatial correlations. VR-CESM shows comparable performance as WRF at 27 km, but still overestimated overall winter precipitation (about 25%-35%) compared to reference datasets, with statistically significant difference over the western edge of the Sierra Nevada, which can be alleviated by increasing the spatial resolution due to improved treatment of orographic effects. The spatial pattern of variability agrees well between VR-CESM and references and when assessing the frequency of strong precipitation events, VR-CESM matched closely to the UW dataset everywhere except the Central Valley.

242 CESM at 1 degree resolution was also assessed in order to better understand the impacts of reso-
243 lution. We find that precipitation patterns over complex topography are poorly represented without
244 capturing the spatial patterns induced by orographic effects over the Cascades and Sierra Nevada
245 by uniform CESM at 1 degree, with total precipitation greatly underestimated, when compared to
246 VR-CESM, gridded data and reanalysis (see the supplement). Basically, the precipitation has been
247 smooth out at the coastal area and the mountainous regions over northwest U.S when simulated
248 with CESM at coarse resolution. This result clearly captures the benefits of high resolution (par-
249 ticularly the representation of topography) in simulating precipitation features. Results are also
250 provided for the output from a globally uniform CESM run at 0.25° spatial resolution with the
251 finite volume (FV) dynamical core (Wehner et al. 2014), exhibiting comparable performance to
252 VR-CESM (see the supplement).

253 (For the t-test among different time periods, I use the yearly values of each run.)

254 **5. Drivers of climatological precipitation**

255 Precipitation has been observed and modeled to being changed regionally and globally under
256 climate warming as discussion in the introduction part.

257 [To be filled in based on earlier discussion based on the literature]

258 [Increased temperatures will lead to higher water vapor content over the ocean, in accordance
259 with C-C. Evaporation over the ocean will increase, but may be limited over land due to limitations
260 on soil moisture. The storm track may be enhanced, which would increase large-scale precipitation
261 events (ARs) along the U.S. west coast.]

262 **6. Results**

263 *a. Mean climatology*

264 Before proceeding with the analysis of precipitation features, it is first important to understand
265 how the mean climatology changes in VR-CESM across time periods (Figure 4). Since the charac-
266 ter of WUS precipitation has a strong seasonal dependence, the mean climatology including mean
267 precipitation, near-surface temperature and near-surface relative humidity are depicted in two sea-
268 sons including the cool season (or wet season) from October to March and the warm season (or
269 dry season) from April to September.

270 As a result of enhanced GHG concentrations, mean annual temperature increases by about 1.5 to
271 2 K from hist to mid and about 4 to 6 K from mid to end. Despite the large spatial variation in cli-
272 matological temperatures, the temperature change between historical and future is fairly uniform.
273 However, there is a slightly weaker increase in the near-coastal regions during cool season and in
274 the lower latitude area at warm season, which might be due to the increased westerly wind during
275 cool seasons and northward wind during warm season from the near ocean. Larger increases of
276 temperature is also observed in warm season than cool season for about 0.5 K and 1 K for mid and
277 end respectively.

278 As described by the Clausius-Clapeyron (C-C) equation, the water vapor content is supposed
279 to increase by $\sim 7\%$ for each 1°C increase in temperature. With the increase of the temperature
280 in future, water vapor evaporation will increase over the ocean. Practically, whether the increase
281 rate of the water vapor as the temperature goes up will keep the same or not will directly affect
282 the relative humidity. As water vapor reaches saturation, condensation triggers clouds and precip-
283 itation. However, when the air holds more water vapor, the chances of heavy rain events tend to
284 increase even when even where total precipitation is decreasing (Trenberth 2011). To understand
285 the increasing rate of water vapor content under climate warming and whether relative humidity
286 can be remain or not, 2m relative humidity (RH) is plotted in Figure 4.

287 Overall, RH remains almost the same as `hist` over the regions where temperature does not sub-
288 stantially increase. However, in regions where temperature increase is larger than 2 K, RH is
289 instead observed to decrease significantly relative to historical values for about 2% and 3-6%
290 compared to `mid` and `end` respectively. In fact, trends in RH are spatially consistent with tempera-
291 ture increase but opposite in magnitude with a spatial correlation coefficient of approximately 0.8.
292 This suggests that continental evaporation and water vapor transport is insufficient to compensate
293 for the air vapor capacity when temperature increases to certain level, which is consistent with
294 Joshi et al. (2008), and has been observed in results by Rowell and Jones (2006) over continental
295 and southeastern Europe and Simmons et al. (2010) over low-latitude and midlatitude land areas.

296 Based on those background changes of heat and water vapor, from `hist` to `mid`, mean precipita-
297 tion showed a 0.2-0.6 mm/day increase during cool season with a largest change over northwest
298 and less than 0.2 mm/day during warm season over southeast part. From `hist` to `end`, the in-
299 crease is about 0.4-1.2 mm/day during cool season with also a largest change over northwest, and
300 no notable change is observed during warm season. Nonetheless, these results are statistically
301 significant (see Figure 5) (how about add significance here)? East of the Rockies, precipitation
302 increases through mid-century (statistically significant), but this trend appears to recede towards
303 the end of the century (although these results are not significant). There is also a decrease of about
304 0.1mm/day in total precipitation over the western flank of the Sierra Nevadas during the cool sea-
305 son from `hist` to future. This decrease (about 0.15 mm/day) is also found over the Cascades and
306 the western coastal area during warm season from `hist` to `mid`. However, this decrease is not sta-
307 tistically significant. Majority of the precipitation over the cool season emerged from large-scale
308 patterns, whereas warm season precipitation was from convection processes.

309 The precipitation over WUS for moderate or heavy precipitation is mainly resulted from the
310 large-scale water flux transport from the eastern Pacific Ocean rather than directly from evapora-

311 tion, mainly in the form of atmospheric rivers or orographic updraft (??). According to previous
312 studies (e.g. (Allan and Soden 2008; ?; Min et al. 2011)), changes in more extreme precipitation
313 follow the C-C relationship more closely than total precipitation precipitation amount (?). In order
314 to find out the precipitation changes in a comprehensive aspect based on our fine-scale simulations,
315 analyses of different precipitation distributions are focused in the following part to account for the
316 future changes of diverse precipitation events.

317 *b. Precipitation indices*

318 We now turn our attention to the precipitation indices presented in Table 1. For each index,
319 the changes of precipitation character for each period, averaged over all ensemble members are
320 plotted in Figure 5 (for the indices that quantify precipitation days) and Figure 6 (for the indices
321 describing precipitation amounts). Although mean precipitation shows a weak but overall increasing
322 trend from `hist` to `mid` and `mid` to `end`, the precipitation indices exhibit substantially more
323 unique character.

324 When comparing `hist` to `mid`, the total rainy days and frequency of non-extreme precipitation
325 have significantly increased mainly over the central-east and southeast part of WUS, which is
326 not observed between `mid` and `end`. On the contrary, the total rainy days and frequency of non-
327 extreme precipitation have decreased significantly over the northwest region and the eastern part
328 of the Montana, Wyoming and Oregon from `mid` to `end`. These changes are the primary driver for
329 the observed change to mean precipitation exhibited in Figure 4.

330 As for extreme precipitation frequency (i.e. days with daily Pr between 10 mm and 40 mm),
331 the number of days increases from `hist` to `mid`, but the pattern is scattered over northwest and
332 central WUS. When comparing `mid` to `end`, there is a clear and significant increase in extreme
333 precipitation events over the northwest coastal area and eastern flank of the Cascades. This result

334 is consistent with Dominguez et al. (2012), who observe a robust increase in winter precipitation
335 extremes toward the latter half of the 21st century using RCMs [an ensemble of RCMs?].

336 There is a slight, but insignificant decrease over the Cascades and the Sierra Nevada (significance
337 is low due to the high variability of precipitation)[Huang: ?]. For very extreme precipitation
338 ($Pr >= 40$ mm) events, there is an increasing trend over the northwest coast and the Cascades
339 and its eastern flank. The corresponding changes in rain amount are consistent with the changes
340 of frequency (see Figure 6). Overall, these results indicate more extreme precipitation over the
341 northwest U.S.

342 (might add the specific percentages for further illustrations)

343 [Why does Fig. 8 appear before Fig. 7?] In order to understand the drivers behind the observed
344 changes, we first examine change in moisture flux for cool seasons when WUS precipitation is
345 primarily from water vapor influx from the Pacific Ocean (see Figure 8). Examining the moisture
346 flux at 850 hPa, we observe an increase in specific humidity that accompanies the increase of the
347 temperature in future [where is this observed? not in Fig. 8]. However, when comparing to hist,
348 wind patterns in mid and end are also reduced over the eastern part of the WUS and enhanced
349 to the west [where? I don't see it]. [These previous several sentences require some clarification
350 as I don't see what you are referring to] Integrated vapor transport (IVT) (Figure 8) for extreme
351 precipitation days over cool seasons. Generally, IVT is useful to understand extreme precipitation
352 events that arise from atmospheric rivers over the northwestern U.S. and from orographic uplift
353 (especially for very extreme precipitation) (Ralph et al. 2004; Leung and Qian 2009; Dettinger
354 2011). Based on the observed change in IVT, it is clear that the increase in moisture influx from
355 past to future, which is mainly due to the change of the air water vapor content with increased
356 temperature, corresponds to the changes of precipitation extremes shown in Figure 5.

357 1) QUANTILE CORRELATION ANALYSIS

358 To see if changes in mean precipitation can be used to predict changes in extreme precipitation
359 features, the correlations between Pr and specific quantiles have been calculated. Here, selected
360 quantiles including the values at 70% (70p), 80% (80p), 90% (90p), 95% (95p) and 99% (99p)
361 are applied based on the all the daily precipitation data at each grid point within each time period.
362 These quantiles are chosen in order to account for the changes of both moderation and extreme
363 precipitation. The mean Pr and those quantiles for hist, and the differences of these quantities
364 among different time periods can be found in the supplemental figure. Within expectation, re-
365 gions with higher Pr are attributed with larger values of those quantiles, i.e. stronger precipitation
366 extremes.

367 Spatial correlation is assessed by computing Pearson product-moment coefficient of linear corre-
368 lation between relevant variables. It is found that the absolute changes of Pr in future are positively
369 related with the absolute changes of the quantiles. This relationship is at a moderate level between
370 mid and hist (larger than 0.65), and becomes stronger when going to the end period (reaching
371 ~0.96). Consistently, the mean Pr itself is also positively correlated with the absolute changes of
372 the quantiles in future (around 0.5 to 0.78), except 70p between end and mid and 99p mid and
373 hist.

374 The relative changes of quantiles are also related with the relative changes of Pr with correla-
375 tions around 0.65 to 0.85, except 70p and 80p between end and mid. So, the area featured with
376 higher increase of extreme precipitations in future also tends to have larger increase of its mean
377 precipitation. However, the wetter area does not necessary have more intense changes of moderate
378 and extreme precipitation than drier area.

379 **might remove 70p**

380 2) ISOLATING DIFFERENCES DUE TO CLIMATE CHANGE AND ENSO

381 [Motivate] The phase of ENSO is well known to have important repercussions on precipitation
382 extremes [citation needed]. ENSO from past to future, the difference of precipitation behaviors
383 between the warm phase (i.e. El Niño) and cool phase (i.e. La Niña) of ENSO is illustrated in
384 Figure 7 for the wet seasons of each time period. Based on the ONI index values, the mean SST
385 anomalies are 1.38, 1.71 and 2.30 K during El Niño years, and -1.16, -1.62 and -1.43 K during La
386 Niña years for hist, mid and end respectively [some references are needed to place this behavior
387 of ENSO within the context of the literature – are these values reasonable?]. The SST anomalies
388 of each year or each month [or?], and their associated spatial pattern when averaged during the
389 warm and cool phases can be found in the supplement (might adding some descriptions of these).

390 [Also include mean SSTs during each period]

391 [Fig. 7 shows a pronounced impact of ENSO through Northern California that seems uncharac-
392 teristic of what I know about ENSO from the literature. I had thought ENSO primarily impacts
393 Southern California. Discuss briefly?]

394 During the El Niño phase, intensified mean precipitation is expected over the southwest (Hamlet
395 and Lettenmaier 2007), along with reduced precipitation intensity over the northwest. This feature
396 is characterized as a northwest/southwest precipitation dipole, triggered by ENSO's modification
397 of the storm track (Gershunov and Barnett 1998; Leung et al. 2003b), along with [?] modula-
398 tion of the enhanced precipitation variability in the southern WUS (Cayan et al. 1999; Kahya and
399 Dracup 1994). This dipole is also apparently in the frequency of rainy days and extreme precip-
400 itation events. In mid and hist, ENSO is observed to intensify, which appears to be related with
401 the changes of the strength of El Niño and La Niña [Since ENSO behavior is strongly dependent
402 on choice of climate model, you need to put this behavior in context and explain how a weakening

403 ENSO could potentially impact these precipitation projections, which should emerge from the lin-
404 ear model result]. This can be explained by the SST anomaly magnitude (detrended) of warm and
405 cold phases (see the supplement). DeFlorio et al. (2013) also found a statistically significant link-
406 ages with ENSO and PDO for both the overall and extreme intensity of wintertime precipitation
407 over the WUS using CCSM4 (earlier form of CESM). Strengthening storm patterns associated
408 with ENSO are also found by Maloney et al. (2014) over California using CMIP5 output under
409 RCP8.5.

410 [Do you want to discuss your observation of only a weak influence from PDO?]

411 [You should show the results of climatological change with changes due to ENSO removed]
412 (For Figure 7, might add percentage of changes)

413 The impact of ENSO is further observed by the IVT difference over rainy days between El Niño
414 and La Niña (see Figure 8) accompanying by the wind pattern difference at 850 hPa, showing
415 the increase of the moisture flux for the southwest and decrease for the northwest. However, the
416 impact of ENSO for observational precipitation has a weaker signal of the dipole effect compared
417 to the VR-CESM (see the supplement), which might suggest that the model has a overestimation
418 of ENSO's impact on precipitation, especially over the northwest U.S. The improvement of ENSO
419 in the model is directly proportional to the representation of ENSO forced precipitation anomalies
420 (AchutaRao and Sperber 2006).

421 Based on the above results, it can be seen that the magnitude of the effects of ENSO is compara-
422 ble or even higher than the impacts of climate forcing. For further investigation, linear regression
423 is applied to signaling the factor effects due to ENSO and climate forcing. First, we get the SST
424 anomaly of each year at each grid point over our study area followed by the way of Niño 3.4 to
425 be the ENSO factor values. Then, we use the GHGs values at each year to represent the climate
426 forcing factor. The features of the precipitation indices as we defined above are used as response

427 variables. Combined the values of all the time period and all the runs, we got the significance of
428 these two factors' effects at each grid point based on the ANOVA (analysis of variance) output.
429 (see the supplement) (This is not complete yet, but not sure whether to add this or not).

430 add the correlation of the quantiles result here

431 7. Discussion and Summary

432 In this study, the North Pacific Oscillation (NPO) is not analyzed as its decadal duration making
433 it difficult to capture within the 26 years simulation time period. Further, as argued by Pierce
434 (2002), the NPO does not [Huang: does not?] respond to the same internal atmospheric variability
435 as ENSO, and so no significant improvement [improvement in what?] can be obtained to account
436 for the ENSO's effects by incorporating accurate predictions of NPO SSTs.

437 The associated precipitation signal under a warmer climate is more ambiguous for California
438 (Neelin et al. 2013) considering the extreme variability on interannual time scales (Dettinger
439 2011). Kim (2005) found that under global warming, heavy precipitation events show largest
440 increases in the mountainous regions of the northern California Coastal Range and the Sierra
441 Nevada. However, our results show a minor decrease (though not statistically significant) of ex-
442 treme precipitation over the Sierra Nevada.

443 Although, the strength of ENSO intensifies in the future with CESM, there is still substantial
444 uncertainty regarding how El Niño will change under global warming by altering the background
445 climate or not as debated by plenty of studies (Fedorov and Philander 2000; Guilyardi et al. 2009)
446 [??]. There is still no clear agreement among coupled models whether ENSO will weaken or
447 strengthen in response to increased greenhouse gas concentrations, particularly as ENSO appears
448 to be relatively insensitive to a doubling of CO₂ in most models (DiNezio et al. 2012). However,
449 correctly simulation changes to the spatial pattern of SSTs ion state-of-the-art coupled GCMs re-

450 mains challenging Joseph and Nigam (2006); Jha et al. (2014); Taschetto et al. (2014). Capotondi
451 (2013) showed that the diversity of El Niño characteristics in CCSM4 is comparable to what was
452 found in observations, although, as found by Deser et al. (2012c), the overall magnitude of ENSO
453 in CCSM4 is overestimated by 30% over the preindustrial time period. Stevenson et al. (2012)
454 assessed ENSO in CCSM4 (predating CESM) and observed no signal when comparing the twen-
455 tieth and twenty-first-century ensembles, as also argued by Philip and Van Oldenborgh (2006). It
456 is believed that large ensembles are needed to isolate a significant climate change response within
457 ENSO, and inter-model teleconnection differences (Stevenson 2012) [?].

458 The increased cool season precipitation extremes tend to result in higher runoff events over
459 the northwest U.S., which are in turn associated with a greater chance of flooding and a loss of
460 snowpack. A decrease in counts of rainy days during the warm season over central and southern
461 California, though small in magnitude, will probably intensify the drought condition due to the
462 deficit of soil moisture with higher evapotranspiration caused by the warmer climate in the future
463 Cayan et al. (2010); Bell et al. (2004).

464 (Summary is to be added once the main content have been settled down)

465 *Acknowledgments.* The authors would like to thank Michael Wehner for sharing the dataset and
466 many suggestions. The authors also want to thank Alan M. Rhoades for providing the simulation
467 output. We acknowledge the substantial efforts behind the datasets used in this study, including
468 UW, NCDC and NARR. The simulation data used is available by request at xyhuang@ucdavis.edu.
469 This project is supported in part by the xxx and by the xxx.

470 References

471 AchutaRao, K., and K. R. Sperber, 2006: Enso simulation in coupled ocean-atmosphere models:
472 are the current models better? *Climate Dynamics*, **27** (1), 1–15.

- 473 Allan, R. P., and B. J. Soden, 2008: Atmospheric warming and the amplification of precipitation
474 extremes. *Science*, **321** (5895), 1481–1484.
- 475 Bell, J. L., L. C. Sloan, and M. A. Snyder, 2004: Regional changes in extreme climatic events: a
476 future climate scenario. *Journal of Climate*, **17** (1), 81–87.
- 477 Caldwell, P., 2010: California wintertime precipitation bias in regional and global climate models.
478 *Journal of Applied Meteorology and Climatology*, **49** (10), 2147–2158.
- 479 Capotondi, A., 2013: Enso diversity in the ncar ccm4 climate model. *Journal of Geophysical
480 Research: Oceans*, **118** (10), 4755–4770.
- 481 Cayan, D. R., T. Das, D. W. Pierce, T. P. Barnett, M. Tyree, and A. Gershunov, 2010: Future
482 dryness in the southwest us and the hydrology of the early 21st century drought. *Proceedings of
483 the National Academy of Sciences*, **107** (50), 21 271–21 276.
- 484 Cayan, D. R., K. T. Redmond, and L. G. Riddle, 1999: ENSO and hydrologic extremes in the
485 western United States*. *Journal of Climate*, **12** (9), 2881–2893.
- 486 DeFlorio, M. J., D. W. Pierce, D. R. Cayan, and A. J. Miller, 2013: Western us extreme precipita-
487 tion events and their relation to enso and pdo in ccm4. *Journal of Climate*, **26** (12), 4231–4243.
- 488 Dennis, J., and Coauthors, 2011: CAM-SE: A scalable spectral element dynamical core for the
489 Community Atmosphere Model. *International Journal of High Performance Computing Appli-
490 cations*, 1094342011428142.
- 491 Deser, C., R. Knutti, S. Solomon, and A. S. Phillips, 2012a: Communication of the role of natural
492 variability in future north american climate. *Nature Climate Change*, **2** (11), 775–779.
- 493 Deser, C., A. Phillips, V. Bourdette, and H. Teng, 2012b: Uncertainty in climate change projec-
494 tions: the role of internal variability. *Climate Dynamics*, **38** (3-4), 527–546.

- 495 Deser, C., and Coauthors, 2012c: Enso and pacific decadal variability in the community climate
496 system model version 4. *Journal of Climate*, **25** (8), 2622–2651.
- 497 Dettinger, M., 2011: Climate change, atmospheric rivers, and floods in california—a multimodel
498 analysis of storm frequency and magnitude changes1. Wiley Online Library.
- 499 Diffenbaugh, N. S., J. S. Pal, R. J. Trapp, and F. Giorgi, 2005: Fine-scale processes regulate the
500 response of extreme events to global climate change. *Proceedings of the National Academy of
501 Sciences of the United States of America*, **102** (44), 15 774–15 778.
- 502 DiNezio, P. N., B. P. Kirtman, A. C. Clement, S.-K. Lee, G. A. Vecchi, and A. Wittenberg, 2012:
503 Mean climate controls on the simulated response of enso to increasing greenhouse gases. *Jour-
504 nal of Climate*, **25** (21), 7399–7420.
- 505 Dominguez, F., E. Rivera, D. Lettenmaier, and C. Castro, 2012: Changes in winter precipitation
506 extremes for the western united states under a warmer climate as simulated by regional climate
507 models. *Geophysical Research Letters*, **39** (5).
- 508 Duffy, P., and Coauthors, 2006: Simulations of present and future climates in the western United
509 States with four nested regional climate models. *Journal of Climate*, **19** (6), 873–895.
- 510 Easterling, D. R., G. A. Meehl, C. Parmesan, S. A. Changnon, T. R. Karl, and L. O. Mearns, 2000:
511 Climate extremes: observations, modeling, and impacts. *science*, **289** (5487), 2068–2074.
- 512 Fedorov, A. V., and S. G. Philander, 2000: Is el niño changing? *Science*, **288** (5473), 1997–2002.
- 513 Fox-Rabinovitz, M., J. Côté, B. Dugas, M. Déqué, and J. L. McGregor, 2006: Variable resolution
514 general circulation models: Stretched-grid model intercomparison project (SGMIP). *Journal of
515 Geophysical Research: Atmospheres (1984–2012)*, **111** (D16).

- 516 Fox-Rabinovitz, M. S., G. L. Stenchikov, M. J. Suarez, and L. L. Takacs, 1997: A finite-
517 difference GCM dynamical core with a variable-resolution stretched grid. *Monthly weather*
518 *review*, **125** (11), 2943–2968.
- 519 Frei, C., R. Schöll, S. Fukutome, J. Schmidli, and P. L. Vidale, 2006: Future change of precipita-
520 tion extremes in Europe: Intercomparison of scenarios from regional climate models. *Journal*
521 *of Geophysical Research: Atmospheres (1984–2012)*, **111** (D6).
- 522 Gao, Y., J. Lu, L. R. Leung, Q. Yang, S. Hagos, and Y. Qian, 2015: Dynamical and thermodynami-
523 cal modulations on future changes of landfalling atmospheric rivers over western north america.
524 *Geophysical Research Letters*, **42** (17), 7179–7186.
- 525 Gates, W. L., 1992: AMIP: The Atmospheric Model Intercomparison Project. *Bulletin of the*
526 *American Meteorological Society*, **73**, 1962–1970.
- 527 Gershunov, A., and T. P. Barnett, 1998: Interdecadal modulation of enso teleconnections. *Bulletin*
528 *of the American Meteorological Society*, **79** (12), 2715–2725.
- 529 Guilyardi, E., A. Wittenberg, A. Fedorov, M. Collins, C. Wang, A. Capotondi, G. J. Van Olden-
530 borgh, and T. Stockdale, 2009: Understanding el niño in ocean-atmosphere general circulation
531 models. *Bulletin of the American Meteorological Society*, **90** (3), 325.
- 532 Hamlet, A. F., and D. P. Lettenmaier, 2005: Production of Temporally Consistent Gridded Precipi-
533 tation and Temperature Fields for the Continental United States*. *Journal of Hydrometeorology*,
534 **6** (3), 330–336.
- 535 Hamlet, A. F., and D. P. Lettenmaier, 2007: Effects of 20th century warming and climate variability
536 on flood risk in the western us. *Water Resources Research*, **43** (6).

- 537 Hegerl, G. C., F. W. Zwiers, P. A. Stott, and V. V. Kharin, 2004: Detectability of anthropogenic
538 changes in annual temperature and precipitation extremes. *Journal of Climate*, **17** (19), 3683–
539 3700.
- 540 Huang, X., A. M. Rhoades, P. A. Ullrich, and C. M. Zarzycki, 2016: An evaluation of the vari-
541 able resolution-cesm for modeling California's climate. *Journal of Advances in Modeling Earth*
542 *Systems*.
- 543 Hurrell, J. W., J. J. Hack, D. Shea, J. M. Caron, and J. Rosinski, 2008: A new sea surface temper-
544 ature and sea ice boundary dataset for the Community Atmosphere Model. *Journal of Climate*,
545 **21** (19), 5145–5153.
- 546 Hurrell, J. W., and Coauthors, 2013: The community earth system model: A framework for col-
547 laborative research. *Bulletin of the American Meteorological Society*, **94** (9), 1339–1360.
- 548 Jha, B., Z.-Z. Hu, and A. Kumar, 2014: Sst and enso variability and change simulated in historical
549 experiments of cmip5 models. *Climate dynamics*, **42** (7-8), 2113–2124.
- 550 Joseph, R., and S. Nigam, 2006: Enso evolution and teleconnections in ipcc's twentieth-century
551 climate simulations: Realistic representation? *Journal of Climate*, **19** (17), 4360–4377.
- 552 Joshi, M. M., J. M. Gregory, M. J. Webb, D. M. Sexton, and T. C. Johns, 2008: Mechanisms for
553 the land/sea warming contrast exhibited by simulations of climate change. *Climate Dynamics*,
554 **30** (5), 455–465.
- 555 Kahya, E., and J. A. Dracup, 1994: The influences of type 1 el nino and la nina events on stream-
556 flows in the pacific southwest of the united states. *Journal of Climate*, **7** (6), 965–976.
- 557 Kao, H.-Y., and J.-Y. Yu, 2009: Contrasting eastern-pacific and central-pacific types of enso.
558 *Journal of Climate*, **22** (3), 615–632.

- 559 Kharin, V. V., F. W. Zwiers, X. Zhang, and G. C. Hegerl, 2007: Changes in temperature and
560 precipitation extremes in the IPCC ensemble of global coupled model simulations. *Journal of*
561 *Climate*, **20** (8), 1419–1444.
- 562 Kim, J., 2005: A projection of the effects of the climate change induced by increased co2 on
563 extreme hydrologic events in the western us. *Climatic Change*, **68** (1-2), 153–168.
- 564 Laprise, R., and Coauthors, 2008: Challenging some tenets of regional climate modelling. *Meteo-*
565 *rology and Atmospheric Physics*, **100** (1-4), 3–22.
- 566 Leung, L. R., L. O. Mearns, F. Giorgi, and R. L. Wilby, 2003a: Regional climate research: needs
567 and opportunities. *Bulletin of the American Meteorological Society*, **84** (1), 89–95.
- 568 Leung, L. R., and Y. Qian, 2009: Atmospheric rivers induced heavy precipitation and flooding in
569 the western US simulated by the WRF regional climate model. *Geophysical research letters*,
570 **36** (3).
- 571 Leung, L. R., Y. Qian, and X. Bian, 2003b: Hydroclimate of the western United States based on
572 observations and regional climate simulation of 1981-2000. Part I: Seasonal statistics. *Journal*
573 *of Climate*, **16** (12), 1892–1911.
- 574 Maloney, E. D., and Coauthors, 2014: North american climate in cmip5 experiments: part iii:
575 assessment of twenty-first-century projections*. *Journal of Climate*, **27** (6), 2230–2270.
- 576 Maurer, E., A. Wood, J. Adam, D. Lettenmaier, and B. Nijssen, 2002: A long-term hydrologically
577 based dataset of land surface fluxes and states for the conterminous United States*. *Journal of*
578 *climate*, **15** (22), 3237–3251.
- 579 McDonald, A., 2003: Transparent boundary conditions for the shallow-water equations: testing in
580 a nested environment. *Monthly weather review*, **131** (4), 698–705.

581 Meehl, G. A., H. Teng, and G. Branstator, 2006: Future changes of el niño in two global coupled
582 climate models. *Climate Dynamics*, **26** (6), 549–566.

583 Mesinger, F., and K. Veljovic, 2013: Limited area NWP and regional climate modeling: a test
584 of the relaxation vs Eta lateral boundary conditions. *Meteorology and Atmospheric Physics*,
585 **119** (1-2), 1–16.

586 Mesinger, F., and Coauthors, 2006: North American regional reanalysis. *Bulletin of the American*
587 *Meteorological Society*, **87**, 343–360.

588 Min, S.-K., X. Zhang, F. W. Zwiers, and G. C. Hegerl, 2011: Human contribution to more-intense
589 precipitation extremes. *Nature*, **470** (7334), 378–381.

590 Neale, R. B., and Coauthors, 2010a: Description of the NCAR community atmosphere model
591 (CAM 5.0). *NCAR Tech. Note NCAR/TN-486+STR*.

592 Neale, R. B., and Coauthors, 2010b: Description of the NCAR Community Atmosphere Model
593 (CAM 5.0). NCAR Technical Note NCAR/TN-486+STR, National Center for Atmospheric Re-
594 search, Boulder, Colorado, 268 pp.

595 Neelin, J. D., B. Langenbrunner, J. E. Meyerson, A. Hall, and N. Berg, 2013: California winter
596 precipitation change under global warming in the coupled model intercomparison project phase
597 5 ensemble. *Journal of Climate*, **26** (17), 6238–6256.

598 NOAA, 2013: Defining El Niño and La Niña. Accessed: 2015-
599 08-20, [https://www.climate.gov/news-features/understanding-climate/
600 watching-el-nio-and-la-nia-noaa-adapts-global-warming](https://www.climate.gov/news-features/understanding-climate/watching-el-nio-and-la-nia-noaa-adapts-global-warming).

- 601 Oleson, K., and Coauthors, 2010: Technical description of version 4.0 of the Community Land
602 Model (CLM). NCAR Technical Note NCAR/TN-478+STR, National Center for Atmospheric
603 Research, Boulder, Colorado, 257 pp. doi:10.5065/D6FB50WZ.
- 604 Philip, S., and G. J. Van Oldenborgh, 2006: Shifts in enso coupling processes under global warm-
605 ing. *Geophysical Research Letters*, **33** (11).
- 606 Pierce, D. W., 2002: The role of sea surface temperatures in interactions between enso and the
607 north pacific oscillation. *Journal of climate*, **15** (11), 1295–1308.
- 608 Ralph, F. M., P. J. Neiman, and G. A. Wick, 2004: Satellite and caljet aircraft observations of
609 atmospheric rivers over the eastern north pacific ocean during the winter of 1997/98. *Monthly*
610 *Weather Review*, **132** (7), 1721–1745.
- 611 Rauscher, S. A., E. Coppola, C. Piani, and F. Giorgi, 2010: Resolution effects on regional climate
612 model simulations of seasonal precipitation over Europe. *Climate dynamics*, **35** (4), 685–711.
- 613 Rauscher, S. A., T. D. Ringler, W. C. Skamarock, and A. A. Mirin, 2013: Exploring a Global
614 Multiresolution Modeling Approach Using Aquaplanet Simulations. *Journal of Climate*, **26** (8),
615 2432–2452.
- 616 Rhoades, A. M., X. Huang, P. A. Ullrich, and C. M. Zarzycki, 2015: Characterizing Sierra Nevada
617 snowpack using variable-resolution CESM. *Journal of Applied Meteorology and Climatology*,
618 **(2015)**.
- 619 Riahi, K., and Coauthors, 2011: RCP 8.5A scenario of comparatively high greenhouse gas emis-
620 sions. *Climatic Change*, **109** (1-2), 33–57.
- 621 Rowell, D. P., and R. G. Jones, 2006: Causes and uncertainty of future summer drying over europe.
622 *Climate Dynamics*, **27** (2-3), 281–299.

- 623 Salathé Jr, E. P., R. Steed, C. F. Mass, and P. H. Zahn, 2008: A High-Resolution Climate Model
624 for the US Pacific Northwest: Mesoscale Feedbacks and Local Responses to Climate Change*.
625 *Journal of Climate*, **21** (21), 5708–5726.
- 626 Scoccimarro, E., M. Zampieri, A. Bellucci, A. Navarra, and Coauthors, 2013: Heavy precipitation
627 events in a warmer climate: results from CMIP5 models. *Journal of climate*.
- 628 Seneviratne, S. I., and Coauthors, 2012: Changes in climate extremes and their impacts on the
629 natural physical environment. *Managing the risks of extreme events and disasters to advance*
630 *climate change adaptation*, 109–230.
- 631 Sillmann, J., V. Kharin, F. Zwiers, X. Zhang, and D. Bronaugh, 2013: Climate extremes indices
632 in the cmip5 multimodel ensemble: Part 2. future climate projections. *Journal of Geophysical*
633 *Research: Atmospheres*, **118** (6), 2473–2493.
- 634 Simmons, A., K. Willett, P. Jones, P. Thorne, and D. Dee, 2010: Low-frequency variations
635 in surface atmospheric humidity, temperature, and precipitation: Inferences from reanalyses
636 and monthly gridded observational data sets. *Journal of Geophysical Research: Atmospheres*,
637 **115** (D1).
- 638 Singh, D., M. Tsiang, B. Rajaratnam, and N. S. Diffenbaugh, 2013: Precipitation extremes over the
639 continental United States in a transient, high-resolution, ensemble climate model experiment.
640 *Journal of Geophysical Research: Atmospheres*, **118** (13), 7063–7086.
- 641 Staniforth, A. N., and H. L. Mitchell, 1978: A variable-resolution finite-element technique for
642 regional forecasting with the primitive equations. *Monthly Weather Review*, **106** (4), 439–447.
- 643 Stevenson, S., 2012: Significant changes to enso strength and impacts in the twenty-first century:
644 Results from cmip5. *Geophysical Research Letters*, **39** (17).

- 645 Stevenson, S., B. Fox-Kemper, M. Jochum, R. Neale, C. Deser, and G. Meehl, 2012: Will there
646 be a significant change to el niño in the twenty-first century? *Journal of Climate*, **25** (6), 2129–
647 2145.
- 648 Taschetto, A. S., A. S. Gupta, N. C. Jourdain, A. Santoso, C. C. Ummenhofer, and M. H. England,
649 2014: Cold tongue and warm pool enso events in cmip5: mean state and future projections.
650 *Journal of Climate*, **27** (8), 2861–2885.
- 651 Taylor, M. A., 2011: Conservation of mass and energy for the moist atmospheric primitive equa-
652 tions on unstructured grids. *Numerical Techniques for Global Atmospheric Models*, Springer,
653 357–380.
- 654 Tebaldi, C., K. Hayhoe, J. M. Arblaster, and G. A. Meehl, 2006: Going to the extremes. *Climatic
655 change*, **79** (3-4), 185–211.
- 656 Trenberth, K. E., 2011: Changes in precipitation with climate change. *Climate Research*, **47** (1),
657 123.
- 658 Wehner, M. F., 2013: Very extreme seasonal precipitation in the NARCCAP ensemble: model
659 performance and projections. *Climate Dynamics*, **40** (1-2), 59–80.
- 660 Wehner, M. F., R. L. Smith, G. Bala, and P. Duffy, 2010: The effect of horizontal resolution
661 on simulation of very extreme US precipitation events in a global atmosphere model. *Climate
662 dynamics*, **34** (2-3), 241–247.
- 663 Wehner, M. F., and Coauthors, 2014: The effect of horizontal resolution on simulation qual-
664 ity in the Community Atmospheric Model, CAM5.1. *J. Model. Earth. Sys.*, doi:10.1002/
665 2013MS000276.

- 666 Yoon, J.-H., S. S. Wang, R. R. Gillies, B. Kravitz, L. Hipps, and P. J. Rasch, 2015: Increasing
667 water cycle extremes in California and in relation to ENSO cycle under global warming. *Nature*
668 *communications*, **6**.
- 669 Zarzycki, C. M., C. Jablonowski, and M. A. Taylor, 2014: Using Variable-Resolution Meshes
670 to Model Tropical Cyclones in the Community Atmosphere Model. *Monthly Weather Review*,
671 **142** (3), 1221–1239.
- 672 Zarzycki, C. M., C. Jablonowski, D. R. Thatcher, and M. A. Taylor, 2015: Effects of localized grid
673 refinement on the general circulation and climatology in the Community Atmosphere Model.
674 *Journal of Climate*, **(2015)**.
- 675 Zhang, X., L. Alexander, G. C. Hegerl, P. Jones, A. K. Tank, T. C. Peterson, B. Trewin, and
676 F. W. Zwiers, 2011: Indices for monitoring changes in extremes based on daily temperature and
677 precipitation data. *Wiley Interdisciplinary Reviews: Climate Change*, **2** (6), 851–870.
- 678 Zhang, X., J. Wang, F. W. Zwiers, and P. Y. Groisman, 2010: The influence of large-scale climate
679 variability on winter maximum daily precipitation over North America. *Journal of Climate*,
680 **23** (11), 2902–2915.
- 681 update the mesh grid plot
- 682 update the plot with new label levels

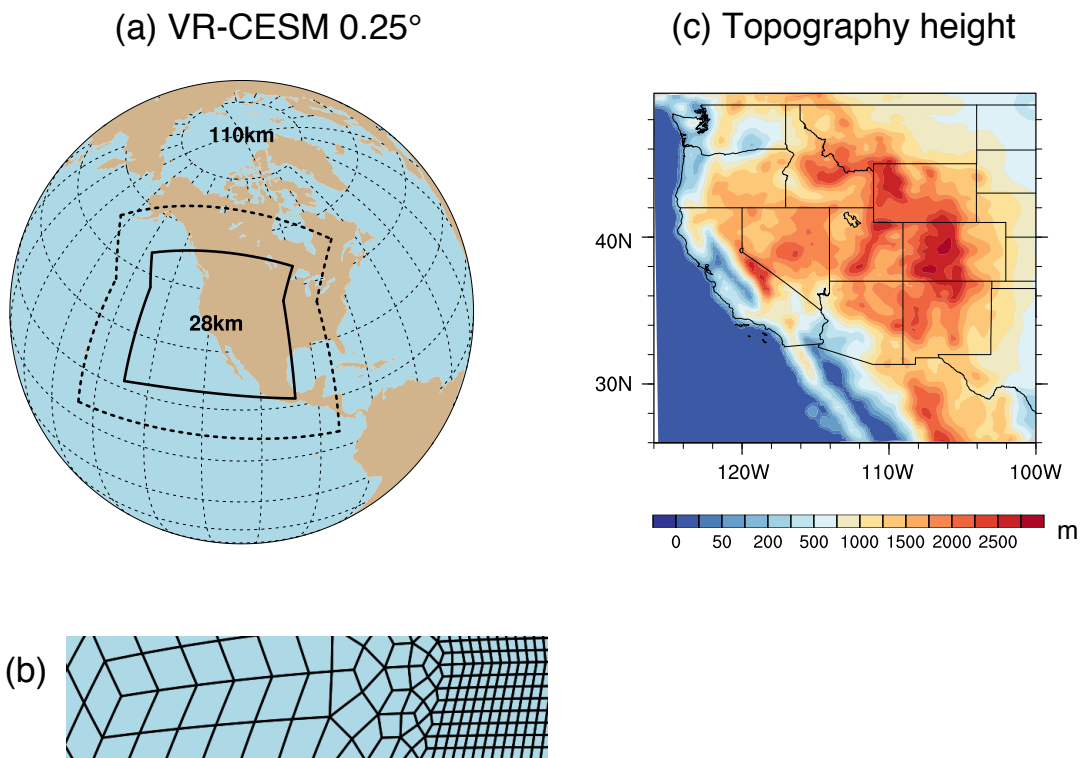
683 LIST OF TABLES

TABLE 1. Precipitation indices employed in this study.

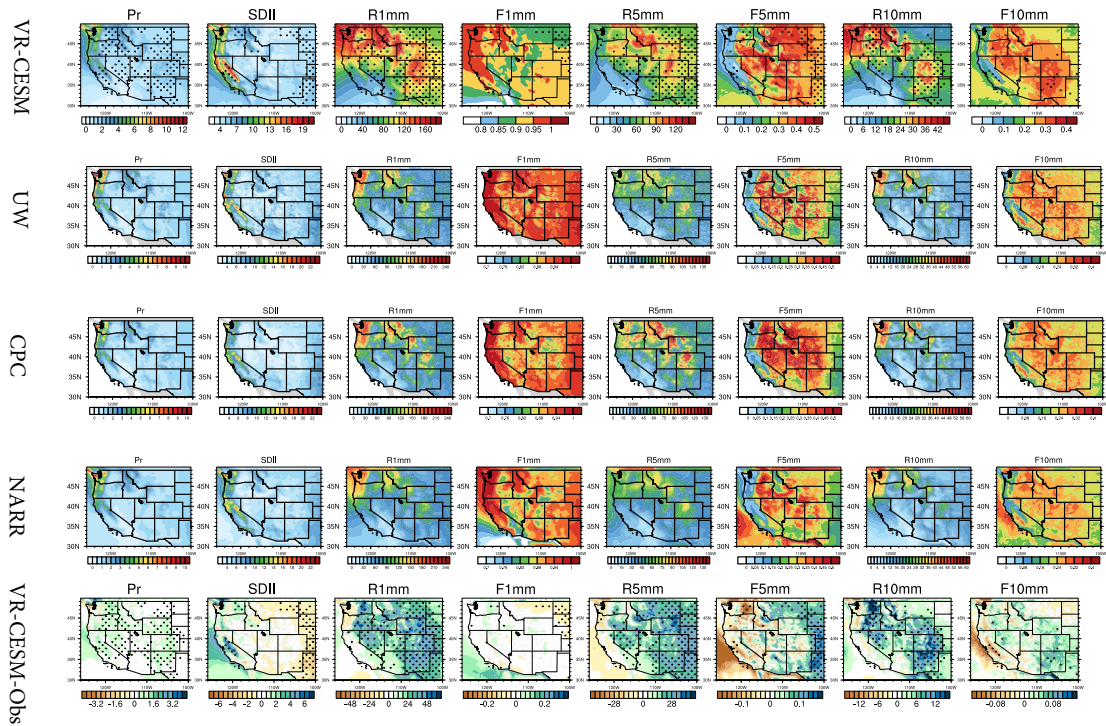
Name	Definition
Pr	Mean daily precipitation
R1mm	Number of days per year with Pr>1 mm
SDII	Simple precipitation intensity index: Precipitation amount / $\langle R1mm \rangle$ (mm/day)
R5mm	Number of days per year with Pr>1 mm and Pr=<5 mm
R10mm	Number of days per year with Pr>5 mm and Pr=<10 mm
R20mm	Number of days per year with Pr>10 mm and Pr=<20 mm
R40mm	Number of days per year with Pr>20 mm and Pr=<40 mm
Rxmm	Number of days per year with Pr>40 mm
F1mm	Fraction of precipitation contributed to the total precipitation for days of R1mm (similarly for F5mm, F10mm, F20mm, F40mm and Fxmm)
P5mm	Precipitation amount from R5mm (similarly for P10mm, P20mm, F40mm, Pxmm)

685 **LIST OF FIGURES**

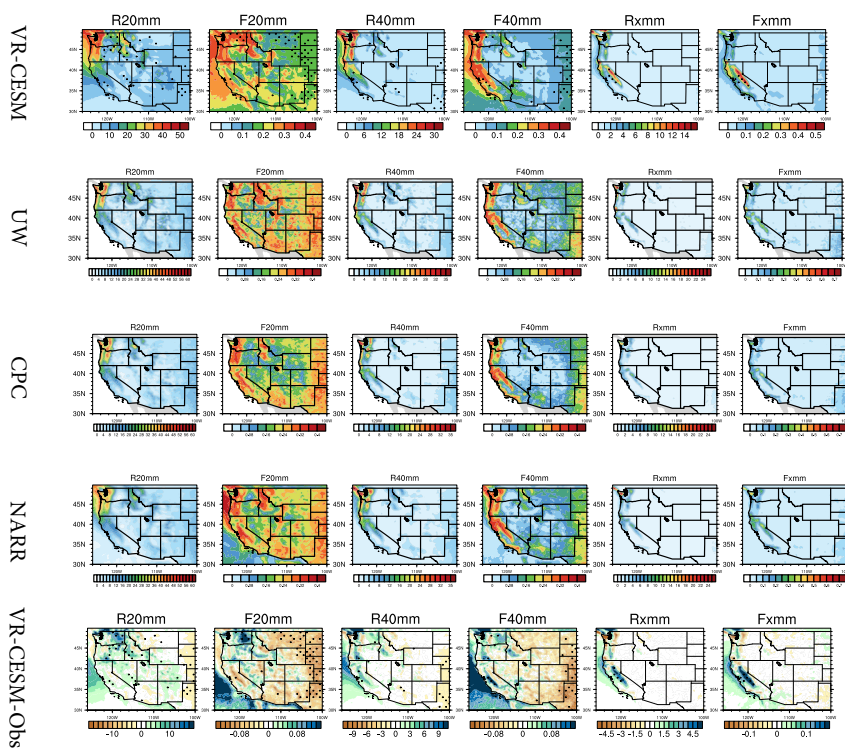
686 Fig. 1.	(a) The approximate grid spacing used for the VR-CESM 0.25° mesh. (b) A depiction of 687 the transition from the global 1° resolution mesh through two layers of refinement to 0.25° . 688 (c) Topography height over the study area.	36
689 Fig. 2.	The mean precipitation and other related indices from VR-CESM and reference datasets 690 over 1980-2005. (Note: Grids with statistically significance difference are marked with 691 stippling.)	37
692 Fig. 3.	The mean precipitation and other related indices from VR-CESM and reference datasets 693 over 1980-2005 (continued).	38
694 Fig. 4.	The mean precipitation (Pr), 2m average temperature ($T2avg$), and 2m relative humidity 695 (RH) averaged over each time period. (Note: Grids with statistically significance difference 696 for the RH are marked with stippling.)	39
697 Fig. 5.	Differences of precipitation behaviors from past to future over WUS averaged of each time 698 period. (Note: Grids with statistically significance difference are marked with stippling.)	40
699 Fig. 6.	Differences of precipitation behaviors from past to future over WUS averaged of each time 700 period (continued).	41
701 Fig. 7.	Difference of precipitation behaviors between warm and cool phases of ENSO from past to 702 future over WUS averaged of each time period.	42
703 Fig. 8.	Changes of moisture flux at 850hPa, and IVT for simulations under different time period 704 and different phases of ENSO of wet season (October to March). (Note: The minimum 705 wind vector is set to be 0.5 m/s, therefore, the wind less than 0.5 m/s is also plotted at 706 the minimum length for better visualization.) For all difference plots, make sure to use 707 a common [min,max] range as its currently difficult to tease out differences. Difference 708 plots should also use a different color table to the mean results (perhaps a single color color 709 table?). Remember that hectopascals is capitalized as hPa.	43



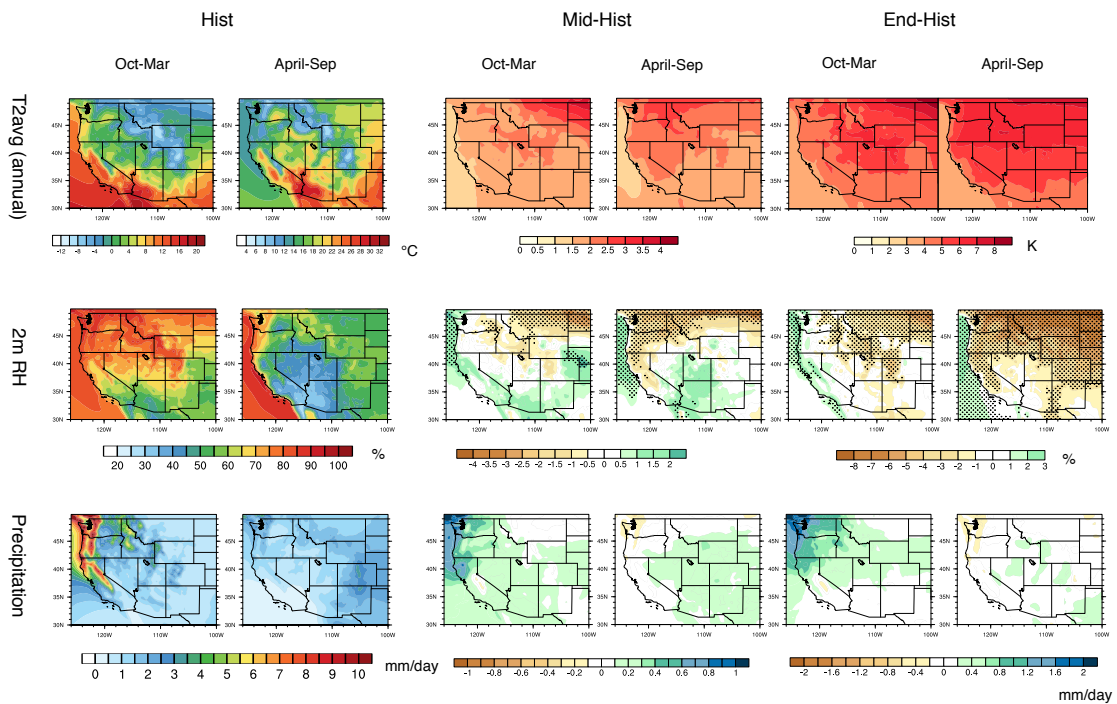
710 FIG. 1. (a) The approximate grid spacing used for the VR-CESM 0.25° mesh. (b) A depiction of the transition
 711 from the global 1° resolution mesh through two layers of refinement to 0.25° . (c) Topography height over the
 712 study area.



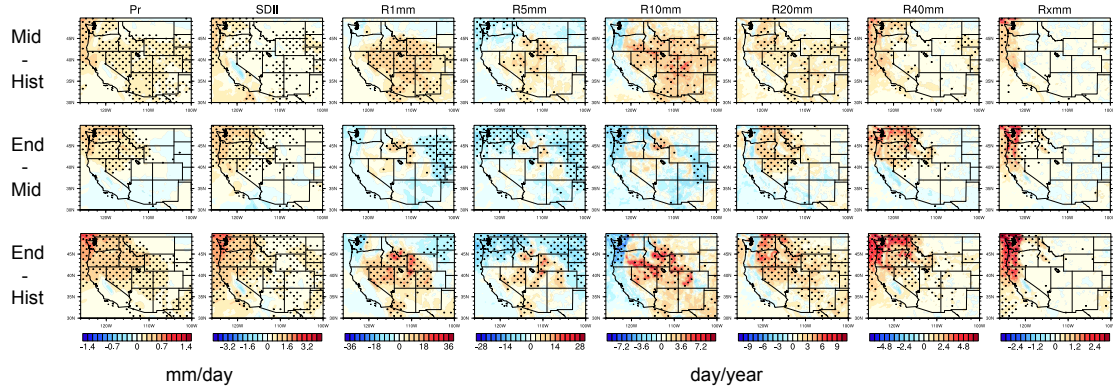
713 FIG. 2. The mean precipitation and other related indices from VR-CESM and reference datasets over 1980-
 714 2005. (Note: Grids with statistically significant difference are marked with stippling.)



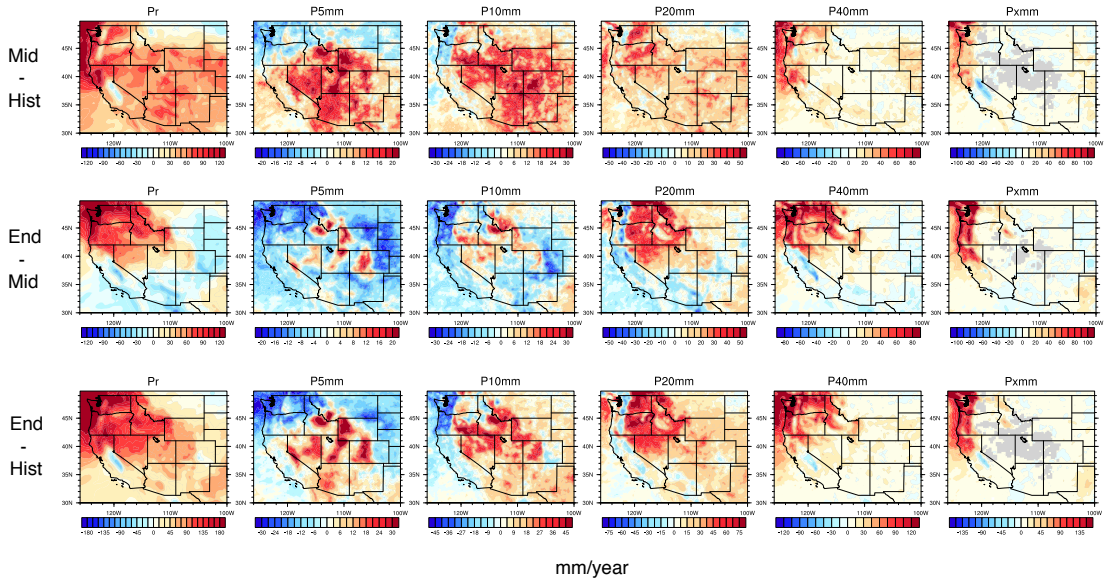
715 FIG. 3. The mean precipitation and other related indices from VR-CESM and reference datasets over 1980-
 716 2005 (continued).



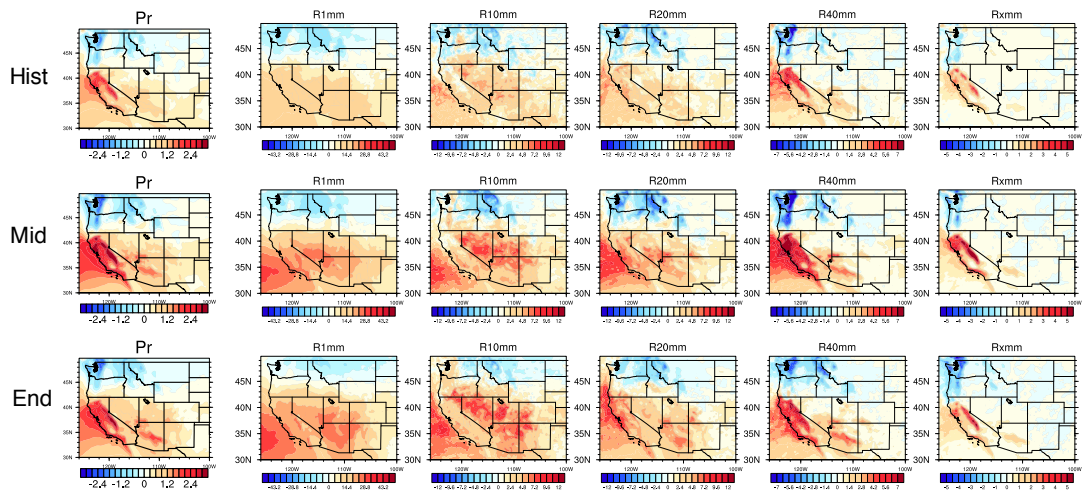
717 FIG. 4. The mean precipitation (Pr), 2m average temperature (T2avg), and 2m relative humidity (RH) aver-
 718 aged over each time period. (Note: Grids with statistically significant difference for the RH are marked with
 719 stippling.)



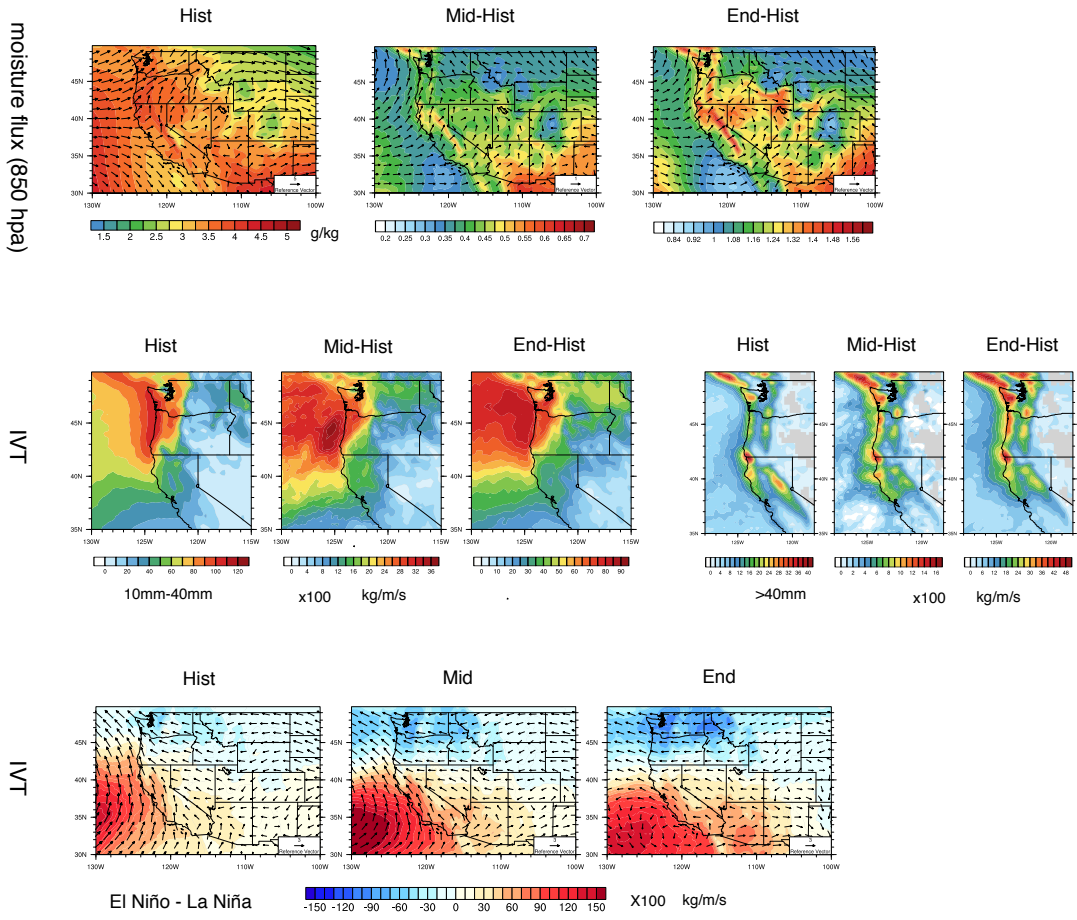
720 FIG. 5. Differences of precipitation behaviors from past to future over WUS averaged of each time period.
 721 (Note: Grids with statistically significance difference are marked with stippling.)



722 FIG. 6. Differences of precipitation behaviors from past to future over WUS averaged of each time period
 723 (continued).



724 FIG. 7. Difference of precipitation behaviors between warm and cool phases of ENSO from past to future
 725 over WUS averaged of each time period.



726 FIG. 8. Changes of moisture flux at 850hPa, and IVT for simulations under different time period and different
 727 phases of ENSO of wet season (October to March). (Note: The minimum wind vector is set to be 0.5 m/s,
 728 therefore, the wind less than 0.5 m/s is also plotted at the minimum length for better visualization.) **For all**
 729 **difference plots, make sure to use a common [min,max] range as its currently difficult to tease out differences.**
 730 **Difference plots should also use a different color table⁴³ to the mean results (perhaps a single color color table?).**
 731 **Remember that hectopascals is capitalized as hPa.**